

Aeroacoustics Investigation of an Uncontrolled and a Controlled Backward-Facing Step with Large Eddy Simulation

Kamil Furkan Taner[1(✉)], Furkan Cosgun[2], and Baha Zafer[2]

[1] Istanbul University, 34315 Avcilar Istanbul, Turkey
furkantaner96@gmail.com
[2] Istanbul Technical University, 34437 Beyoglu Istanbul, Turkey
cosgun15@itu.edu.tr, zaferba@itu.edu.tr

Abstract. In this study, 3D flow over backward-facing step is solved for low Mach number. Large Eddy Simulation is used to resolve turbulent features into the flow field. Numerical results of turbulent flow field are compared with experimental velocity profiles for different stations and those are validated. Additional to accounting a flow field, sound levels for different located receivers due to backward-facing step flow are determined using Acoustic Analogy (AA) which is firstly proposed by Lighthill. Unsteady flow field variables obtained from computational fluid dynamics commercial code is used as input in Ffowcs Williams-Hawkings (FW-H) Equation, which is an extended version of Lighthill equation. Additionally, some active flow control methodologies are carried out to a flow field to understand better relations between flow controls and acoustic results. These flow control techniques are the suction and blowing with different magnitudes at the bottom of backward-facing step. The controlled cases are also compared with experimental flow field results and validated. Acoustic results are plotted in frequency and time domain. Different active control effects on acoustic results are evaluated and interpreted.

Keywords: Backward-facing step flow · Large eddy simulation · Acoustic analogy · Low mach number · Flow control

1 Introduction

The Backward Facing-Step (BFS) flow is a popular research topic to understand of separated and reattaching flow situations, despite of its simplicity [1]. The Backward-Facing Step (BFS) flows are also called "sudden expansion flow", "diverging channel" or "backward flow" [2]. Due to that the backward-facing step (BFS) is available in many engineering applications and structures, it has been being a significant subject. Gas transport systems, aerospace applications

© Springer Nature Switzerland AG 2020
O. Gervasi et al. (Eds.): ICCSA 2020, LNCS 12250, pp. 503–517, 2020.
https://doi.org/10.1007/978-3-030-58802-1_36

(i.e. aircraft landing systems of aircraft, weapon bays on aircrafts), marine equipment designs, environmental applications (i.e. entrance of harbours, air flow in canyon streets), industrial applications (i.e. wind movements around high-rise buildings), automotive equipments (i.e. automobile's pillars, car sunroofs) are essential engineering problems where the flow of the backward-facing step is investigated [3].

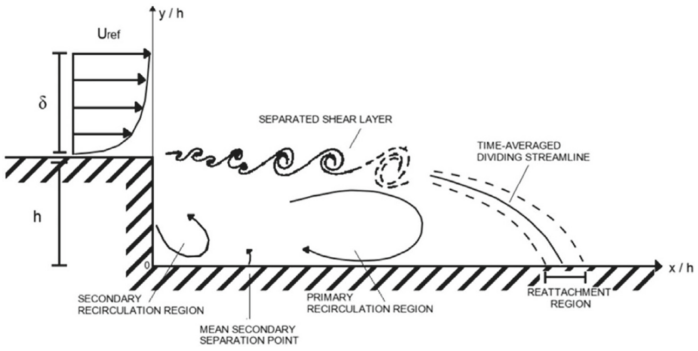

Fig. 1. Nature of backward-facing step flow [4].

Generally, the BFS flow field is divided into four regions: separated shear layer, the primary and secondary recirculation region under the shear layer and the reattachment region. In terms of flow dynamics, the BFS flow occurs with large separation vortices and with some small vortex in the corner (secondary recirculation region) as shown in Fig. 1 [2]. Flow separation from the step edge leads to high speed eddies, large energy losses, vibration and noises [5]. In the last few years, both flow control techniques, the suction and blowing [6,7], not only became interesting research areas in fluid mechanics, but also affected techniques which have a significant role in aeroacoustics. In the literature, the essential part of the experimental and numerical studies has been investigated for high Reynolds and Mach numbers. On the other hand, studies for low Mach number has not been carried out so much. Zheng et al. [5] studied BFS flow with continuous suction and without control by using the turbulence model of LES. The effects of suction control on the flow field were studied for different suction velocities and the results showed that the suction is effective in shortening the reattachment length, reducing the tangential velocity gradients and turbulence fluctuations of reattachment flows. In the study of Uruba et al. [7]. BFS flow was investigated by suction and blowing while using different slot shapes (rectangle or serrated), slot area and flow coefficient which varies from -0.035 up to 0.035. Results indicate that suction and blowing are able to reduce the length of the separation zone whereas slot shapes and slot areas are significant only for blowing. In this case, small cross-section with serrated edge is the most effective. Neumann and Wengle [1] investigated a passive control approach for an unsteady separated

flow. The objective of the passive control was to enhance the entrainment rate of the shear layer bounding the separation zone behind the step, thereby reducing the mean reattachment length. DNS and LES at $\mathrm{Re}_h = 3000$ were carried out for all flow cases (uncontrolled and controlled). A certain minimum distance between the step edge (h) and the upstream position of the control fence is required to achieve a maximum reduction of the reattachment length. Choi et al. [8] observed BFS flow numerically. All numerical simulations were investigated with RANS and LES turbulence models using open source CFD package OpenFOAM. The numerical investigation has been implemented for various step angles (10°, 15°, 20°, 25°, 30°, 45°, and 90°), different expansion ratios (1.48, 2.00 and 3.27), and Reynolds numbers (5000, 8000, 11000, 15000, 47000 and 64000). As a result, LES shows a better agreement than RANS model. In current study, incompressible flow over backward-facing step for low Mach number has been solved using Large Eddy Simulation. While calculated Reynolds number is 0.0855×10^5 and Mach number is 0.015. Firstly, a mesh independence study has been conducted to determine most efficient mesh size in terms of computational cost and solution's accuracy. Five different mesh sizes have been attempted. After mesh convergence is satisfied, the numerical results for the flow field have been compared and validated with the experimental results. Additional to comparison and validation process, the sound level induced flow over backward-facing step has been determined for different locations using Ffowcs-Williams Hawkings equation. Some active flow control mechanisms have also carried out to observe the effects of flow control on aeroacoustics results. These active flow control mechanisms are flow suction-blowing with different magnitudes from a small slot located at the bottom of the step. The controlled flow field results have also compared with the experimental data and validated. In the light of these right flow field results, the sound level comparisons have been computed and which suction or blowing rate is the most effective or the worst in terms of sound levels have been recognized.

2 Numerical Methods and Aeroacoustics Equations

The computational mechanic commercial flow solver is used for numerically discrete temporal conservation equations, which are related to flow field, using the finite volume method. Bounded Central Differencing Scheme is used for spatial discretization. Second Order Implicit Scheme is used for temporal discretization. In addition to these, the pressure-velocity decoupling of discretised equation is carried out by the PISO (pressure implicit with splitting of operators). Non-Iterative Time Advancement solver is used in order to reduce the computational time. Time step size is set as 0.0004 s. and number of time steps is set 5000. Used equations for LES model are obtained by filtering temporal Navier - Stokes equations. The filtered variable is demonstrated below:

$$\overline{\varphi}(x) = \int_D \overline{\varphi}(x^{'}) G(x, x^{'}) dx^{'} \tag{1}$$

In Eq. (1), "D" represents control volume, "G" is the filter function, which demonstrates resolved eddies scale. Finite volume discretization provides

implicitly processing of filtering. Lighthill transformed continuity and momentum equations to a non-homogenous wave equation that has a source term. It considers only aerodynamically generated sounds without solid body interaction. This approach is known as Acoustic Analogy (AA) in aeroacoustics. In Eq. (2) is the Lighthill equation:

$$\frac{\partial^2 \rho}{\partial t^2} - a_{\infty^2} \frac{\partial^2 \rho}{\partial x_{i^2}} = \frac{\partial^2 T_{ij}}{\partial x_i \partial x_j} \tag{2}$$

Lighthill equations were redefined and generalized, using the generalized function theory, by Ffowcs Williams-Hawkings (FW-H). In Eq. (3) is FW-H equation:

$$\begin{aligned} \frac{1}{a_0}\frac{\partial p^{'}}{\partial t^2} - \nabla p^{'} = {} & \frac{\partial^2}{\partial x_i \partial x_j}\{T_{ij}\ H(f)\} - \frac{\partial}{\partial x_i}\{[P_{ij} n_j + \rho u_i (u_n - v_n)]\}\ \delta\ (f)\} \\ & + \frac{\partial}{\partial t}\{[\rho_0 v_i + \rho u_i (u_n - v_n)\delta(f)]\} \end{aligned} \tag{3}$$

In the FW-H equations, while the left side is the wave equation form, three source terms are used in the right side. These source terms are loading, thickness and quadrupole respectively. In Eq. (3), the first term on the right side is quadrupole, the second term is loading, and the final term is thickness. In Eq. (3), u_i is component of flow velocity magnitude in x_i direction, u_n is component of flow velocity magnitude in normal of solid surface, v_i is component of solid surface velocity magnitude in x_i direction and v_n is component of solid surface velocity magnitude in normal of solid surface. $\delta(f)$ and H(f) are Dirac delta, Heaviside function respectively. p' represents sound pressure in far field and is defined as ($p' = p - p_0$). $f = 0$ also expresses a mathematical surface ($f > 0$) in external flow problem which is in infinite space. This mathematical surface can be defined as a permeable surface in the flow field. Thus, it facilitates the theoretical investigation and generalization of the definition function. In addition, Green function solutions can be used in free space. T_{ij} is Lighthill stress tensor and it is defined in Eq. (4):

$$T_{ij} = \rho u_i u_j + P_{ij} - a_{0^2}(\rho - \rho_0)\delta_{ij} \tag{4}$$

P_{ij} denotes a compressive stress tensor and is given in Eq. (5) for Stoke Flows:

$$P_{ij} = p\delta_{ij} - \mu\left(\frac{\partial u_i}{\partial x_j} + \frac{\partial u_j}{\partial x_i} - \frac{2}{3}\frac{\partial u_k}{\partial x_k}\delta_{ij}\right) \tag{5}$$

Details about the used receiver locations are shown in Fig. 2. Sum, 35 receivers are set up into BFS's different locations. On the BFS's edge (2 microphones) and bottom walls (8 microphones) have 10 receivers totally. Inside of BFS channel, 7 receivers were placed on R = 2h radius circle with 15° angle and 13 microphones are placed on R = 4h with 15° angle. The radius circles centre point is defined at the step edge. Last 5 receivers are 5h away from the bottom wall and parallel to it.

3 Computational Domain and Boundary Conditions

Examined computational domain is shown in Fig. 3. The domain has a slot where the flow is controlled. The computational domain has the rectangular

cross-section. The step height $h = 0.025\,m$, the BFS channel has a length of upstream 16h and the length of downstream is 56h (m). The rectangular cross section has a height 10h and a width of 4h. Velocity at the inlet, the reference velocity, is $U_e = 5\,m/s$. The rectangular slot with the size of $a = 0.95 \times 10^{-3}$ m is studied. More information about this geometry can be found in Uruba et al. [7]. In our study, Mach number (Ma) and Reynolds number (Re_h) of computed flow are 0.015 and 0.0855×10^5 respectively. Multi-block structured and non-uniform orthogonal grids are used to divide the computational domain into finite volume cells. Mesh structure is tightly handled in order to analyse the dynamic vortex structure that occurs immediately front step.

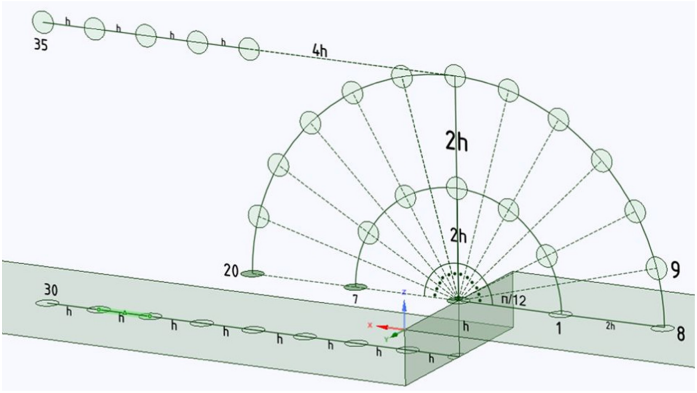

Fig. 2. Location of receivers for BFS geometry.

4 Computational Domain and Boundary Conditions

Examined computational domain is shown in Fig. 3. The domain has a slot where the flow is controlled. The computational domain has the rectangular cross-section. The step height $h = 0.025\,m$, the BFS channel has a length of upstream 16h and the length of downstream is 56h (m).

The rectangular cross section has a height 10h and a width of 4h. Velocity at the inlet, the reference velocity, is $U_e = 5\,m/s$. The rectangular slot with the size of $a = 0.95 \times 10^{-3}$ m is studied. More information about this geometry can be found in Uruba et al. [7]. In our study, Mach number (Ma) and Reynolds number (Re_h) of computed flow are 0.015 and 0.0855×10^5 respectively. Multi-block structured and non-uniform orthogonal grids are used to divide the computational domain into finite volume cells. Mesh structure is tightly handled in order to analyse the dynamic vortex structure that occurs immediately front step. The boundary conditions of BFS geometry are expressed precisely. The velocity profile at the channel inlet and at the slot are set as uniform flow. Therefore, a sufficiently long space (16h) is allowed backflow of the step. Moreover, velocity values do not have any stochastic component and their flows are laminar.

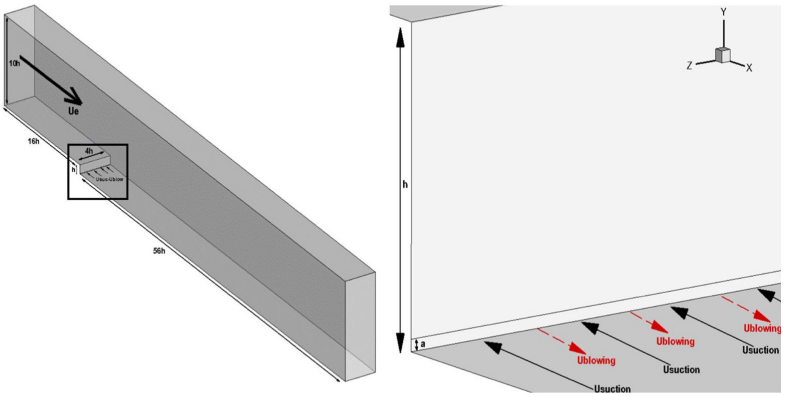

Fig. 3. Computational domain of BFS and slot configuration.

When there is a no suction or no blowing at the slot, the slots are changed to the no-slip wall boundary conditions. A zero gradient condition is used at the outflow. It assumes that the flow field is fully developed at the boundary and the changes in the values in the field are zero at the outflow. The no-slip condition is applied at the rest of the surfaces of the computational domain. Continuous suction and blowing were used at the slot located on the step, and the intensity of the flow control were expressed as C_Q. In Eq. (6), C_Q is described. The C_Q is defined negative for suction and positive for blowing cases.

$$C_Q = \frac{\rho_{s-b} U_{s-b} F_{s-b}}{\rho_e U_e F_e} = \frac{w U_{s-b} a}{w U_e H} = \frac{U_{s-b} a}{U_e H} \tag{6}$$

C_Q is also called the suction and blowing flow coefficient; U_e and F_e are the incoming velocity-flow, which were given from cross-sectional area of channel's inlet; ρ_e is density of incoming air-flow; U_{s-b} and F_{s-b} are the air suction and blowing velocity, which were given from the slot (a); ρ_{s-b} is the density of suction and blowing air. The studied cases with flow control or without control were given in Table 1.

Table 1. Details of studying cases.

Cases	C_Q	$U_{suction}$	$U_{blowing}$
C_0	0	0	0
C_1	−0.01	−13.157	–
C_2	0.01	–	13.157
C_3	−0.035	−46.052	–
C_4	0.035	–	46.052

5 Numerical Results

In the first step, grid independency works are done to investigate optimum mesh size and computational cost. In the numerical studies, ensuring the resolution, accuracy and low computational cost of the solution are crucial. Detailed mesh domain strategy which is used for all mesh sizes is shown in Fig. 4. Therefore, the first step of this section is to include mesh independence tests.

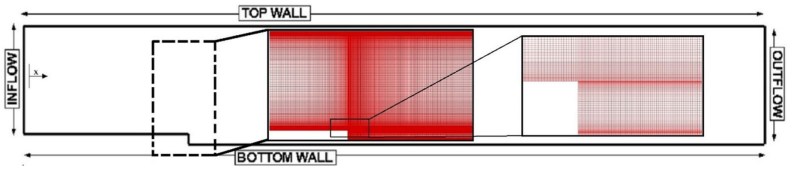

Fig. 4. Meshing strategy of gird-independency work.

Five different cases were generated to obtain the number of mesh size. Total number of elements increase regularly from Case 1 to 5, while the minimum element number is 982 thousand and the maximum number of elements is 4.2 million. When generating mesh structures, we paid attention to maximum aspect ratio of elements. This ratio should not exceed high values. Particularly in the case of turbulent flows, the high aspect ratio value causes divergence.

Table 2. Number of elements of cases used in mesh independency.

Cases	Total number of elements
Mesh 1	*0.982 Million*
Mesh 2	*1.5 Million*
Mesh 3	*2.5 Million*
Mesh 4	*3.3 Million*
Mesh 5	*4.2 Million*

All numerical results, which can be seen in Table 2, for five different cases are compared with the experimental data to define which mesh size is optimum to acquire the best computational cost. The normalised velocity profiles are extracted for different normalised x-direction station after back-step corner, namely $x/h = 2$, 4, 6 and 8. These profiles are shown in Fig. 5. The closing mesh independency study, Case 4 (3.3 million), is chosen as the best nominee for the further computational works.

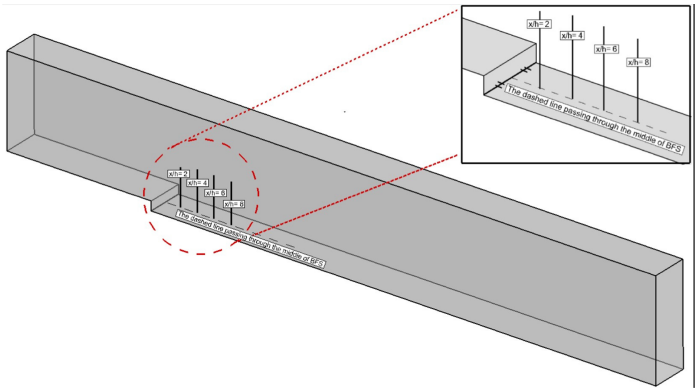

Fig. 5. Four different stations at computational domain.

The results of mesh independency tests are shown in Fig. 6. It is observed that the velocity profiles behave almost the same in all mesh sizes at all four stations. However, it can be said that especially Mesh 4 and 5 give better results at first and second stations (x/h = 2, 4). In addition, almost all mesh sizes show exceptionally good results with the experimental data at third and fourth stations (x/h = 6, 8). In this respect, Mesh 4 is used in the further studies and flow field results are obtained to calculate acoustic measurements by using this mesh. Furthermore, it is evaluated as a base concept.

Figure 7a, 7b, 8a and 8b show more detailed results with respect to time averaged x direction velocity (u) obtained from four stations and pressure distribution taken from the bottom wall after the step. In Fig. 7a, all stations give significantly good results with experimental study. In Fig. 7b, the mean pressure coefficient, C_P, on the bottom wall of the symmetry plane in the x direction is computed from unsteady flow field results and the numerical simulations are compared with the experimental data. Both results gradually increase to reach maximum point which is observed nearly at the point x/h = 8.2. The mean pressure coefficient is defined at the step edge nearly $C_p = -0.18$ for the experimental data and $C_p = -0.16$ for the numerical computation. As it can be seen in Fig. 8, the reattachment point is located at x = 0.11. Low pressure territory occurs before the reattachment point, whereas high pressure territory occurring after the reattachment point.

When looking at Fig. 8a, it can be said that shear layer is starting to be formed at the BFS step and it spreads and its thickness increases. The reattachment point shows itself as a point where the sign of pressure value is changed in Fig. 8b. A careful investigation of the velocity profiles in Fig. 7 reveals that the most deviation

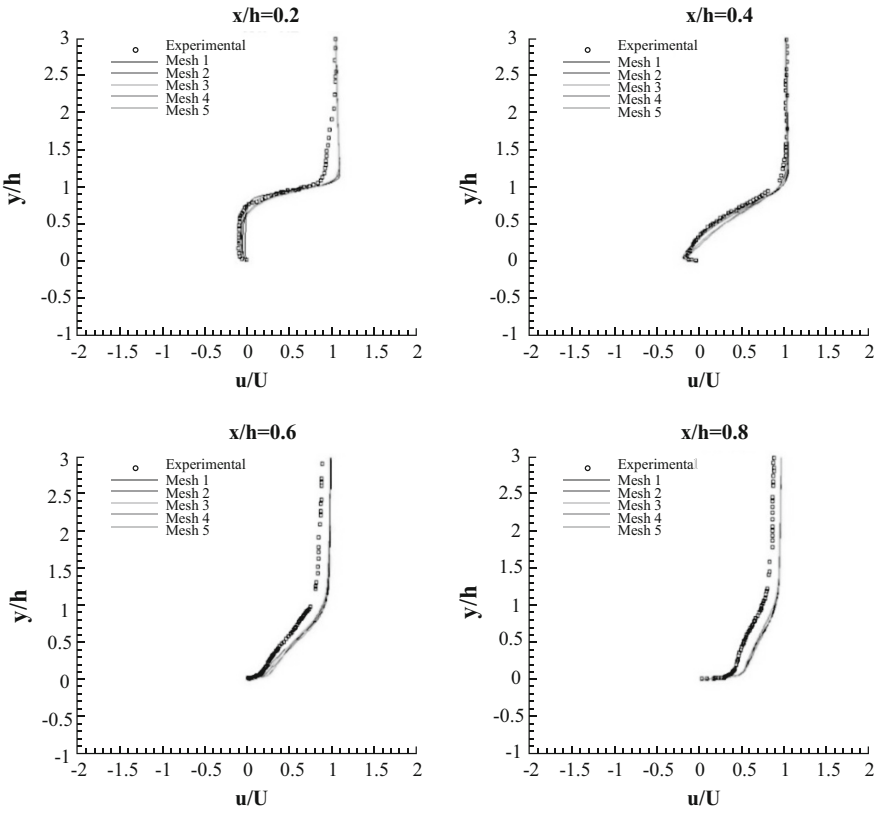

Fig. 6. Mesh independency test results for x direction normalized velocity profile.

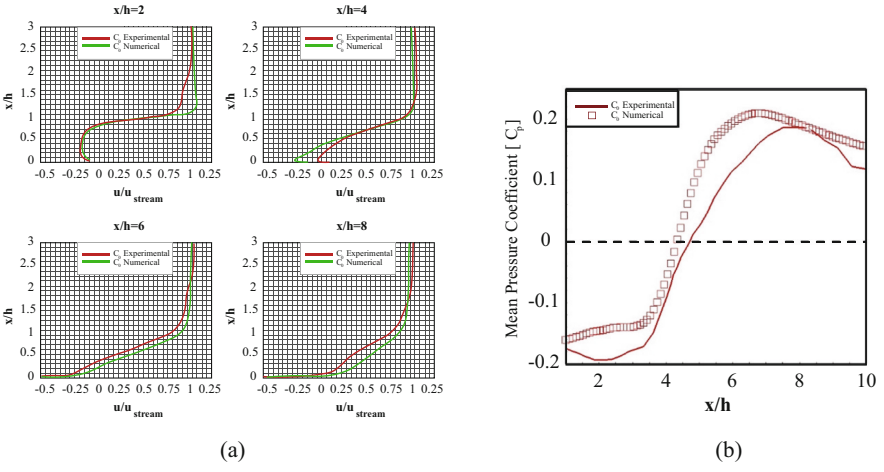

Fig. 7. Comparisons between the experiment and numerical simulation with respect to (a) mean u velocity and (b) mean pressure coefficient.

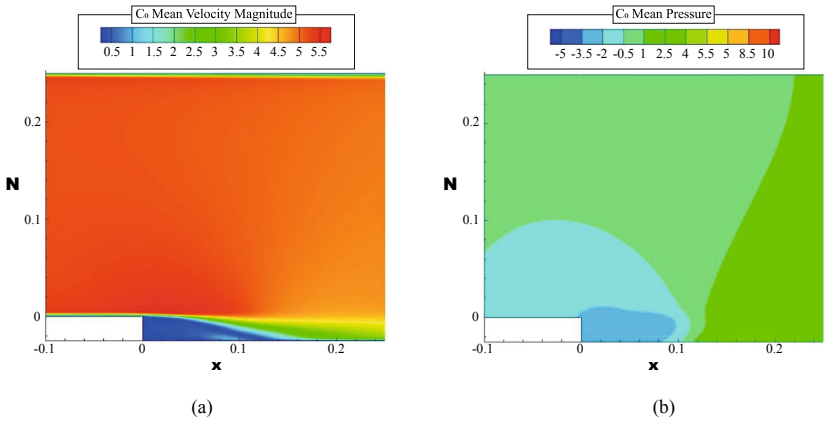

Fig. 8. Time averaged flow field for BFS (a) mean velocity magnitude and (b) mean pressure.

is shown at the reattachment point that is nearly located at x/h = 4 region. The acoustic pressures are calculated by using FW-H acoustic analogy. This anology uses flow field pressure values obtained from the acoustic source surface. The source surface is defined at the bottom wall in this study. As mentioned above, 35 receivers were placed but only the results of three specific microphones are given for practical presentation. These are Receiver 9, 20 and 35.

Figure 9 shows the acoustics results of the receivers induced by flow over Backward-Facing Step (BFS) for C_0. The spectrum for Receiver 20 has the highest sound pressure level (SPL) since it is the nearest microphone to the reattachment point region. On the other hand, Receiver 35 has the lowest sound pressure level while Receiver 9 gives 35 dB and 25 dB sound levels 50 Hz 100 Hz respectively. When investigating the flow field results the fact can be seen that main sound source is appeared in front territory of a step which includes upwind and downwind of the reattachment point that those regions have higher pressure changes over time, Fig. 10. In this respect, it can be said that the nearer to the main source region the higher sound level is imposed. This is the main reason why Receiver 20 shows the highest sound levels. In addition, Receiver 9 and Receiver 35 are located at same distance to main source region but Receiver 9 shows higher values compared to Receiver 35. This may be since Receiver 9 is nearer to a boundary layer region compared to Receiver 35. It is estimated that additional to main source surface noise, higher sound levels in Receiver 9's spectrum has also boundary layer noise (Fig. 13).

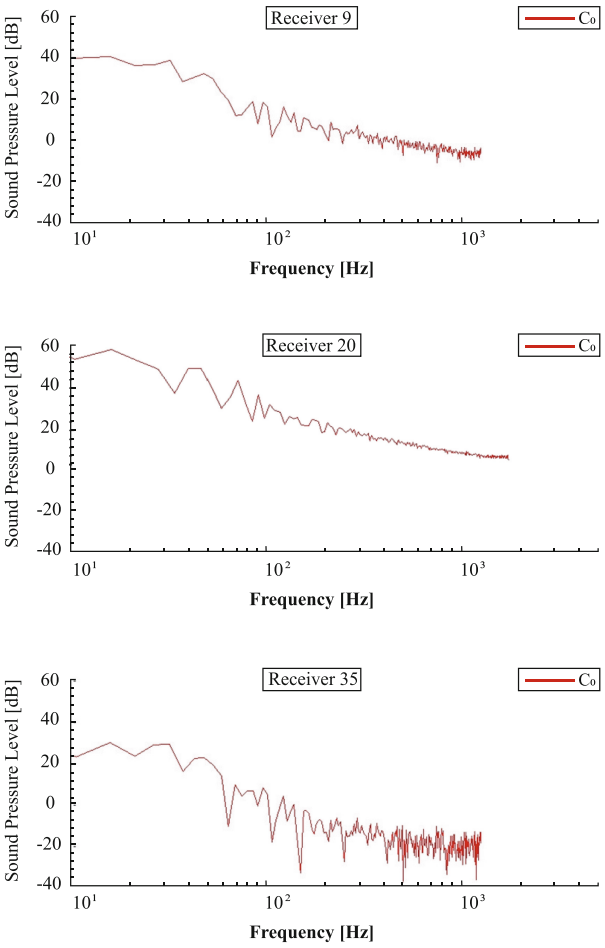

Fig. 9. Acoustics spectrums of bacward facing step for three microphone locations.

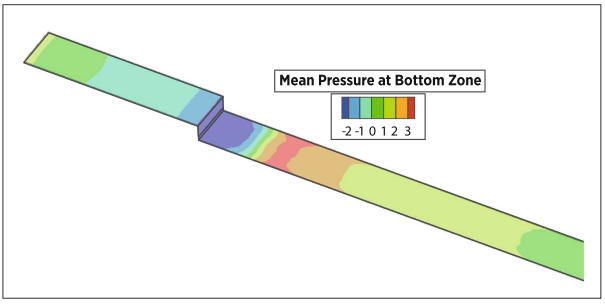

Fig. 10. Pressure distributions on the acoustics source.

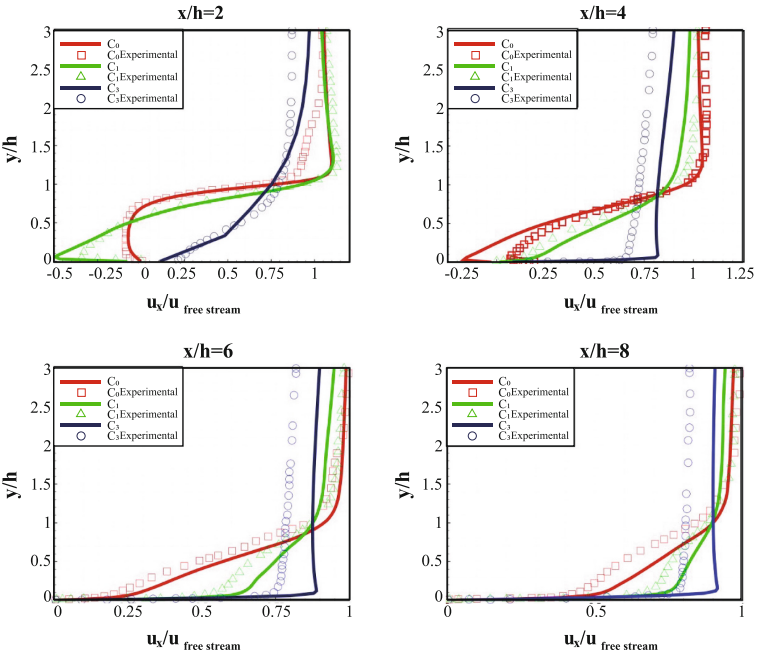

Fig. 11. Velocity profile comparison for C_0, C_1, and C_3 cases.

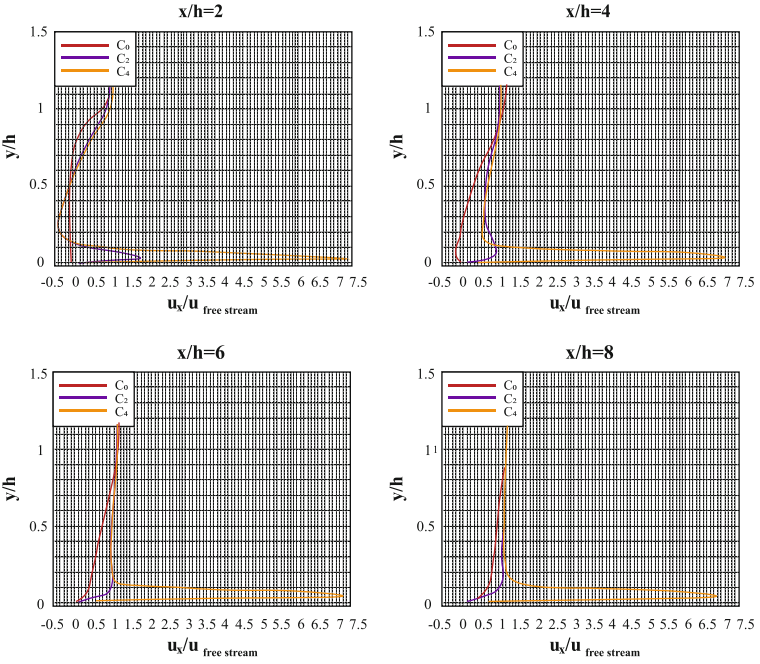

Fig. 12. Velocity profile comparison for C_0, C_2, and C_4 cases.

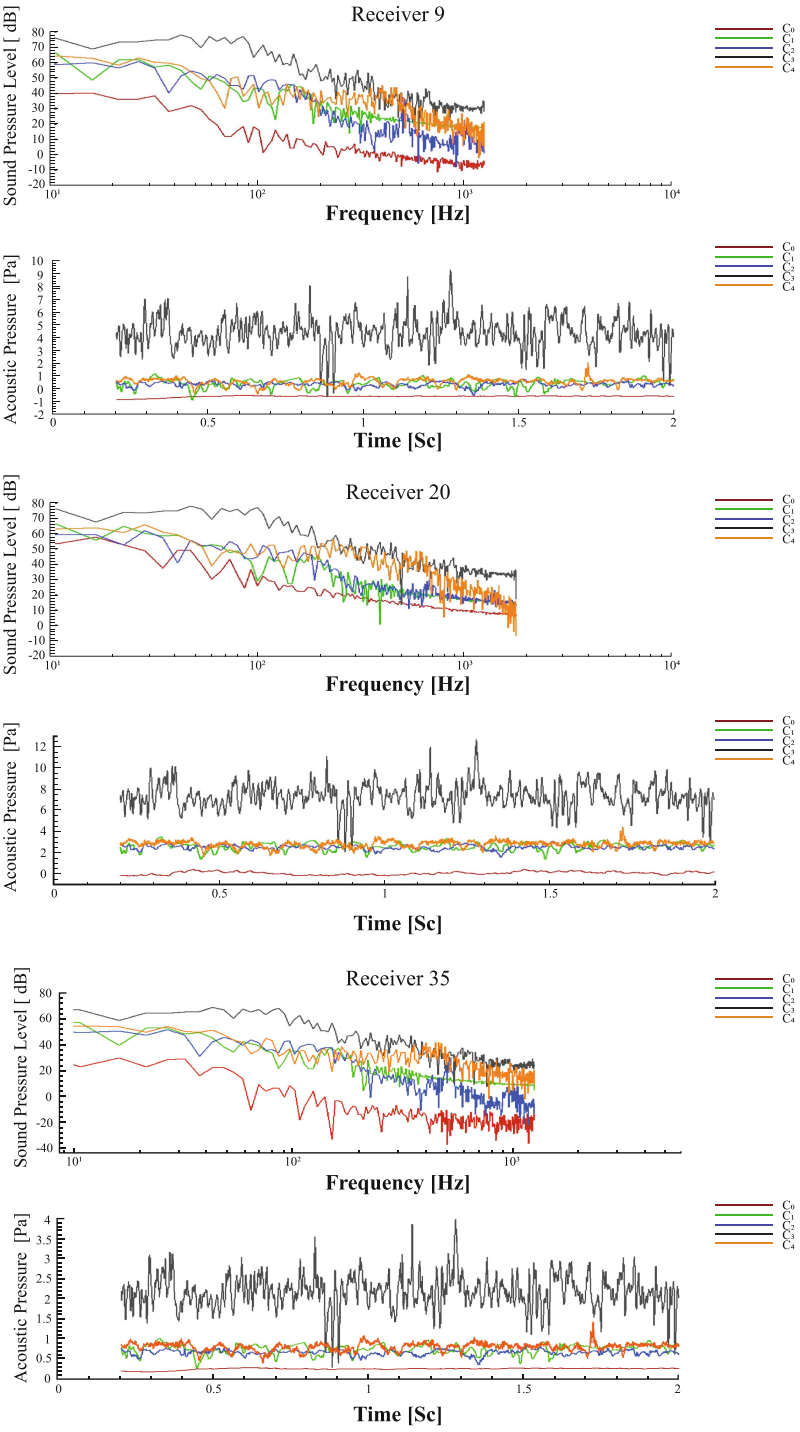

Fig. 13. Aeroacoustics comparisons for different control mechanisms.

6 Conclusion

The geometry of the Backward Facing Step (BFS) causes large energy loses, strong acoustic waves, local pressure, density, and velocity fluctuations. The noise, vibration and undesired acoustic signals due to the structure of BFS geometry can disturb people and decrease ergonomics. Limiting the separation zones, in particular, the recirculation zones, determining to noise levels and reducing them have been crucial so far in fluid mechanics and aeroacoustics researches. Studying a Backward Facing Step (BFS) flow can be applicable to the landing gear cavity problems as well. When the aircraft goes close to the airfield, the landing gear systems swing for landing. At this very moment, Mach number of the aircraft initiates to diminish below 0.2. During this landing operation, landing gear cavity geometry occurs and this cavity geometry is significant for industrial problems and applications. Since the cavity creates huge noises and vibrations. This study can assist to understand this landing gear cavity problem. In the literature, low Mach number studies have not been investigated as much as high Reynold number studies. In this study, the commercial flow solver is used to solve the BFS problem numerically. Large Eddy Simulation approach is applied for better understanding of physics of turbulence, separated/reattached flows and acoustics in the flow field. Ffowcs Williams and Hawkings (FW-H) equation is used as an acoustic model to obtain the noise that is generated by the aerodynamic effects. Totally, 35 receivers set up into the BFS's different locations. These locations are designated with the consideration of the previous studies such as Zafer et al. [9]. The investigated BFS model is taken by Uruba et al. [7]. Flow control techniques (no suction/blowing, suction and blowing situations) are investigated with giving different velocities. First of all, mesh independency works are done to find the best grid system. Thus 5 different mesh structures with a various number of elements are generated. Then, these are compared with each other and the best mesh size is defined. Velocity profiles and mean pressure coefficient (Cp) value are validated between our numerical and experimental results for C_0 case. Cp's experimental value was obtained by Hudy et al. [10]. In addition, the experimental velocity profile values were obtained by Uruba et al. [7]. In the C_0 case, a good agreement is seen between the experimental and numerical results in terms of the velocity profiles, mean pressure coefficient, and reattachment point. After that, different suction velocities were given (Fig. 11) and our numerical results were compared to another numerical study that was done by Zheng et al. [5]. Moreover, the blowing velocities are given (Fig. 12), and their results are added to the study. Finally, for 35 receivers, acoustic results are obtained for all cases (Fig. 13), however; results of receiver 9, 20 and 35 are shared in the study. Receiver 20 is the nearest microphone to the reattachment point region, thus; it is exposed the highest sound pressure. Receiver 9 and 35 are located at same distance to the main source region. Yet, Receiver 9 shows higher values compared to Receiver 35. This result appears since Receiver 9 is nearer to a boundary layer region compared to Receiver 35. It is estimated that additional to main source surface noise, higher sound levels in Receiver 9 spectrum has also boundary layer noise which is radiated from boundary layer

distributions of flow which occurs before the step or it can be called as coming flow. The C_1, C_2 and C_4 cases exhibit a similar behaviour between 10 Hz to around 100 Hz. When frequency value hit to around 200 Hz, C_4 case start to display distinctive behaviour until around 600 Hz. It is also noted that when suction velocity increases, SPL value increases. In conclusion, it is commonly expected that the BFS structure should have reduced recirculation zones and the C_0 case (no suction/blowing) has the longest reattachment length compare to the other cases which is investigated.

Giving suction or blowing velocity from the slot creates reduced recirculation zones. However, this leads reverse situations in terms of acoustic result. Although the C_0 has longest reattachment length, it also has the lowest sound pressure level (SPL) than the other cases. In brief, giving suction or blowing from the slot may shorten reattachment, while increasing the sound pressure level.

References

1. Neumann, J., Wengle, H.: DNS and LES of passively controlled turbulent backward-facing step flow. Flow Turbul. Combust. **71**, 297–310 (2003)
2. Chen, L., Asai, K., Nonomura, T., Xi, G., Liu, T.: A review of Backward-Facing Step (BFS) flow mechanisms, heat transfer and control. Thermal Sci. Eng. Prog. **6**, 194–216 (2018)
3. Ozsoy, E.: Numerical simulation of incompressible flow over a three dimensional rectangular cavity. Ph.D. thesis, Istanbul Technical University (2010)
4. Ruisi, R., Zare-Behtash, H., Kontis, K., Erfani, R.: Active flow control over a backward-facing step using plasma actuation. Acta Astronaut. **126**, 354–363 (2016)
5. Zheng, C.R., Zhang, Y.C., Zhang, W.Y.: Large eddy simulation of separation control over a backward-facing step flow by suction. Int. J. Comput. Fluid Dyn. **25**, 59–73 (2011)
6. Abu-Nada, E., Al-Sarkhi, A., Akash, B., Al-Hinti, I.: Heat transfer and fluid flow characteristics of separated flows ecountered in a backward-facing step under the effect of suction and blowing. J. Heat Transfer **129**, 1517–1528 (2007)
7. Uruba, V., Jonas, P., Mazur, O.: Control of channel-flow behind a backward-facing step by suction/blowing. Int. J. Heat Fluid Flow **28**, 665–672 (2007)
8. Choi, H.H., Nguyen, V.T., Nguyen, J.: Numerical invetigation of backward facing step flow over various step angles. Procedia Eng. **154**, 420–425 (2016)
9. Zafer, B., Cosgun, F.: Aeroacoustics investigation of unsteady incompressible cavity flow. J. Faculty Eng. Archit. Gazi Univ. **31**, 665–675 (2016)
10. Hudy, L.M., et al.: Particle image velocimetry measurements of a two/three-dimensional separating/reattaching boundary layer downstream of an axisymmetric backward-facing step. In. AIAA 43rd Aerospace Sciences Meeting and Exhibit, Reno, Nevada, 10–13 January 2005. AIAA Paper 2005-114 (2005)